CtBP restricts DUX-dependent and -independent genetic program for the 2-cell-like state in murine embryonic stem cells

Kazuma Yoshioka[1], Kota Sugiyama[1], Maki Ichisakino[1], Selma Alamanda Abadi[1], Nao Hayakawa, Miyu Marutani, Ryo Masuda, Kyo Takahashi and Yoshiyuki Seki

Department of Biomedical Sciences, School of Biological and Environmental Sciences, Kwansei Gakuin University, Hyogo, Japan

[1]Co-first author

[*]Correspondence: yseki@kwansei.ac.jp

Abstract

After fertilization, maternally deposited mRNA is cleared, and *de novo* mRNA is transcribed from the zygotic genome through zygotic genome activation (ZGA), a process known as maternal-to-zygotic transition (MZT) occurring in the mouse at 2-cell (2C) stage. 2C-like cells (2CLCs) marked by MERVL expression are transcriptionally similar to 2C embryos spontaneously emerge from mouse embryonic stem cells (mESCs). Although the emergence of 2CLCs completely depends on DUX function, a recent knockout study clearly showed that DUX is dispensable for mouse embryos, suggesting that DUX-independent molecular pathways are not recapitulated in 2CLCs. We present here that the disruption of C-terminal binding protein 1/2 (*Ctbp1/2*) activates DUX-dependent and -independent molecular pathway associated with the development of early mouse embryos mediated by the upregulation of Preferentially expressed antigen of melanoma family-like 7 (PRAMEL7). Furthermore, the abnormality of the gene expression profile caused by *Dux* KO is partially rescued by the overexpression of PRAMEL7 in mESCs. Our study provides new insights into the DUX-independent molecular pathway for the activation of early embryonic genes in mESCs.

33 **Introduction**

34 After fertilization, maternal factors direct development and trigger zygotic genome
35 activation (ZGA) at the around late one-cell stage in mice, called maternal-to-zygotic
36 transition (MZT)(Eckersley-Maslin et al., 2018). The early-cleavage stage embryos
37 acquire cellular totipotency to generate both embryonic proper and extraembryonic
38 tissues during MZT. Although totipotency was thought to be exclusive to the early-
39 cleavage stage embryos, a part of the molecular network is recapitulated in the totipotent-
40 like cells (2-cell-like cells; 2CLCs) marked by the expression of endogenous retrovirus
41 MERVL, which are an endogenous subpopulation of mouse embryonic stem cells (ESCs).
42 (Macfarlan et al., 2012a) (Rodriguez-Terrones et al., 2018).

43 The transition from pluripotent stem cells into 2CLCs is a useful *in vitro* system for
44 identifying the gene regulatory network for ZGA, and several genes that control the
45 emergence of 2CLCs from pluripotent cells have been identified (Eckersley-Maslin et al.,
46 2019; Hu et al., 2020; Ishiuchi et al., 2015; Percharde et al., 2018; Rodriguez-Terrones et
47 al., 2018). The transcription factor DUX (DUX4 in humans) is a critical factor for
48 regulating the transition from pluripotent stem cells into 2CLCs and the expression of
49 ZGA genes (De Iaco et al., 2017; Hendrickson et al., 2017; Whiddon et al., 2017). Ectopic
50 expression of DUX enhances the population of 2CLCs, whereas the *Dux* disruption
51 eliminates the emergence of spontaneous 2CLCs during mESC culture. Several 2CLC
52 regulatory genes have been identified, but they are either direct activators (DPPA2/4, p53
53 and NELFA) or direct repressors (CAF-1, LINE-1 and SETDB1) of *Dux* expression
54 (Eckersley-Maslin et al., 2019; Grow et al., 2021; Ishiuchi et al., 2015; Percharde et al.,

55 2018; Wu et al., 2020). However, both *Dux* zygotic and maternal knockout embryos can
56 survive full-term (Chen and Zhang, 2019; Guo et al., 2019), suggesting that DUX-
57 independent molecular pathways not recapitulated in 2CLCs are critical for ZGA and the
58 early development of mice.

59 In this study, we show that disruption of Ctbp1/2 (C-terminal binding protein 1/2)
60 (Stankiewicz et al., 2014)activates two distinct sets of genes in ESCs: the first set is
61 transiently upregulated in a DUX-dependent manner during minor ZGA, and the second
62 set contains maternally expressed genes and the upregulated genes in a DUX-independent
63 manner during major ZGA. Preferentially Expressed Antigen in Melanoma-like 7
64 (PRAMEL7) is directly upregulated by the loss of *Ctbp1/2* without DUX function, and
65 upregulated PRAMEL7 activates minor ZGA genes in a DUX-dependent manner and
66 maternally expressed genes and major ZGA in DUX-independent manner in mESCs.
67 These data revealed that CtBP restricts the DUX-dependent and -independent genetic
68 programs for the 2-cell-like state in mESCs.

69

70

71 **Material and Methods**

72 **Cell Culture**

73 E14tg2a ESCs (RIKEN Cell Bank) were cultured in Glasgow minimum essential medium
74 (GMEM; Wako) containing 10% fetal calf serum (FCS; Invitrogen), 1 mM glutamine
75 (Wako), nonessential amino acids (Wako) and 500 μM Monothioglycerol Solution
76 (Wako). The culture was supplemented with 1000 U/ml of leukaemia inhibitory factor
77 (LIF) (Wako) without feeder cells. ESCs were cultured in N2B27 medium with 2i
78 (PD0325901, 0.4 μM: WAKO, CHIR99021, 3 μM: Sigma-Aldrich).

79

80 **Generation of knockout ESCs using a CRISPR-Cas9 system**

81 Guide RNAs for *Ctbp1/2*, *Dux* and *Pramel7* were generated in pX330-U6- Chimeric_BB-
82 CBh-hSpCas9 (Addgene plasmid #42230; deposited by Feng Zhang; Cong et al., 2013).
83 The guide RNA sequences are listed in Supplementary Table 1. The pX330 was co-
84 transfected with pCAG-EGFP into E14tg2a with MERVL::TurboGFP (Addgene plasmid
85 #69072; deposited by Maria-Elena Torres-Padilla; (Ishiuchi et al., 2015). The GFP-
86 positive fraction was sorted by Cell Sorter (No. SH800; Sony Biotechnology, Inc., Tokyo,
87 Japan). Genomic DNA deletions were sequenced (Supplementary Figure 1).

88

89 **qRT-PCR and RNA-Seq**

90 Total mRNA was purified with a PureLink^{TM} RNA Mini Kit (Ambion, Inc.). For
91 quantitative RT-PCR, cDNA was synthesized by ReverTra Ace® qPCR RT master Mix
92 (Toyobo), and then analyzed by qPCR with FastStart SYBR Green Master Mix (Roche)

93 using a specific primer set for each gene (Supplementary Table 1). RNA-seq libraries
94 were generated using Collibri™ Stranded RNA library prep for illumina™ Systems
95 (ThermoFisher Scientific) and sequenced using HiSeq X™ Ten (Illumina) (150-bp
96 paired-ends reads).
97
98 **Data analysis of RNA-Seq and public ChIP-seq data**
99 Total mRNA of each cell line was purified with a PureLink™ RNA Mini Kit (Ambion,
100 Inc.) by biological duplicate. RNA-seq libraries were generated using Collibri™ Stranded
101 RNA library prep for illumina™ Systems (ThermoFisher Scientific) and sequenced using
102 HiSeq X™ Ten (Illumina). Reads were aligned by Hisat2 to the Mus musculus genome
103 (mm10). Raw read counts of genes were calculated by R package FeatureCounts using
104 mm10 KnownGenes. GTF from UCSC for annotation. Normalized count data, principal
105 component and K-means clustering analysis were exported by the interactive Expression
106 and Pathway analysis (iDEP) webserver using the count data or normalized expression
107 data of early mouse embryos (Ge et al., 2018). Differentially expressed genes (DEGs)
108 were selected using a cut-off at a false discovery rate (FDR) ≦ 0.1 and a ≧ 2-fold
109 change in expression. Gene set enrichment analysis (GSEA) was used to determine
110 whether upregulated genes by *Ctbp1/2* knockouts were enriched for the upregulated genes
111 in 2-cell embryos or 2CLCs as described previously. Venn diagrams showing overlapping
112 genes were constructed by BioVenn, a web application (Hulsen et al., 2008).
113 Pubic ChIP-seq data for CtBP2 were re-analyzing using GREAT (Genomic Regions
114 Enrichment of Annotations tool) with the "two nearest genes" setting, which assigns each

115 peak to the two closest transcription start sites (TSSs) within 1 Mb. Peak visualization of
116 ChIP-seq peaks for CtBP2, H3K27Ac and DUX was performed using Integrative
117 Genomics Viewer (IGV) (Hendrickson et al., 2017; Kim et al., 2015; McLean et al., 2010;
118 Zhang et al., 2020).
119
120 **Immunofluorescence analysis**
121 Cells were fixed by 4% paraformaldehyde at 4°C for 20 min, followed by incubation with
122 PBS containing 0.5% Triton-X at 4°C for 5 min. Permeabilized cells were incubated with
123 a primary antibody solution containing anti-GFP (Nacarai Tesque, 04404-84, 1:500) with
124 anti-ZSCAN4 (Merk Millipore, AB4340, 1:1000) or anti-MuERVL-Gag (Epigentek, A-
125 2801-050, 1:250) or anti-OCT4 (Santa Cruz, Sc-8628, 1:500) or anti-CtBP2 (BE
126 Biosciences, 612044, 1:500) followed by secondary antibody solution containing anti-
127 Rat IgG Dylight™ 488 antibody (Rockland, 612-141-120, 1:500) or anti-Rabbit IgG
128 Dylight™ 549 antibody (KPL, 042-04-15-06, 1:500) or anti-Mouse IgG Dylight® 550
129 antibody (Abcam, ab96876, 1:500) or anti-Goat IgG Dylight™ 549 antibody (Rockland,
130 605-742-002, 1:500) with 1 μg/ml of DAPI solution (DOJINDO, 340-07971).
131
132 **Luciferase assay**
133 The enhancer candidate region of *Pramel7* or *Dux* was cloned into pGL4.23, driving the
134 *luciferase* gene. Wild-type or *Ctbp1/2* DKO ESCs were transfected with the reported
135 constructs with *Ctbp2* or *Pramel7* expression vector using HilyMax (DOJINDO). Cells
136 were harvested 36 hours after transfection, and the luciferase activities were measured

137 using the Dual-luciferase Reporter Assay System (Promega).

138

139 **Western blotting analysis**

140 Cells were lysed by boiling SDS sample buffer (WAKO). Before lysed proteins were
141 applied to polyacrylamide-SDS gels, 2-mercaptoethanol was added to denature the
142 proteins. The lysed proteins were separated on polyacrylamide-SDS gels, blotted on a
143 polyvinylidene fluoride membrane, and probed using the following primary antibodies:
144 anti-UHRF1 (MBL, D289-3, 1:1000) or anti-TUBLIN (SIGMA, T5168, 1:5000).
145 Following the primary antibody reaction, the membrane were incubated with horseradish
146 peroxidase (HRP)-coupled secondary antibodies. All antibodies were detected with
147 Immunostar LD (WAKO).

148

149 **Phylogenetic tree inference**

150 Amino acid sequences of PRAME family proteins were obtained from Ensemble release
151 112. Multiple-sequence alignment was performed using the ClustalW algorithm with the
152 MEGA software, version 11 with default parameters. Molecular phylogenetic trees were
153 inferred with the maximum-likelihood method using MEGA software, version 11 with
154 default parameters.

155

Results

CtBP1/2 acts as negative regulators of the transition from pluripotent ESCs to two-cell-like cells (2CLCs)

We have previously shown that CtBP1/2 are essential for the transition from formative to naïve pluripotency in mouse embryonic stem cells (mESCs) (Yamamoto et al., 2020). To investigate their roles of CtBP1/2 beyond pluripotency maintenance, we performed RNA sequencing (RNA-seq) to compare the gene expression profiles between wild-type (WT) and *Ctbp1/2* double-knockout (DKO) ESCs. An MA-plot revealed a marked upregulation of two-cell (2C)-specific genes, including *Dux*, *Zscan4* and *Zfp352*, together with repeat elements such as MERVL, MT2 and GSAT_Mm in *Ctbp1/2* DKO ESCs (Figure 1A, B). Gene set enrichment analysis (GSEA) using a reference set of 2C embryo and 2C-like cell (2CLC)-enriched genes (n=404; (Macfarlan et al., 2012)) confirmed a strong enrichment of 2C-related transcripts among those upregulated in the absence of CtBP1/2 (Figure 1C).

To directly monitor the induction of 2CLC state, we generated *Ctbp1/2* DKO ESCs carrying the MERVL-EGFP reporter (Ishiuchi et al., 2015). The GFP-positive fraction was approximately 0.1 % in WT ESC, whereas *Ctbp1/2* DKO ESCs exhibited an over 50-fold increase (7.4%) in GFP-positive cells, indicative of robust 2CLC induction (Figure 1D). These GFP-positive cells co-expressed hallmark 2CLC markers such as ZSCAN4 and MERVL-GAG, while pluripotency-associated factors such as OCT4 were markedly reduced (Figure 1E), consistent with previous reports (Eckersley-Maslin et al., 2016; Zhu et al., 2021).

182

183

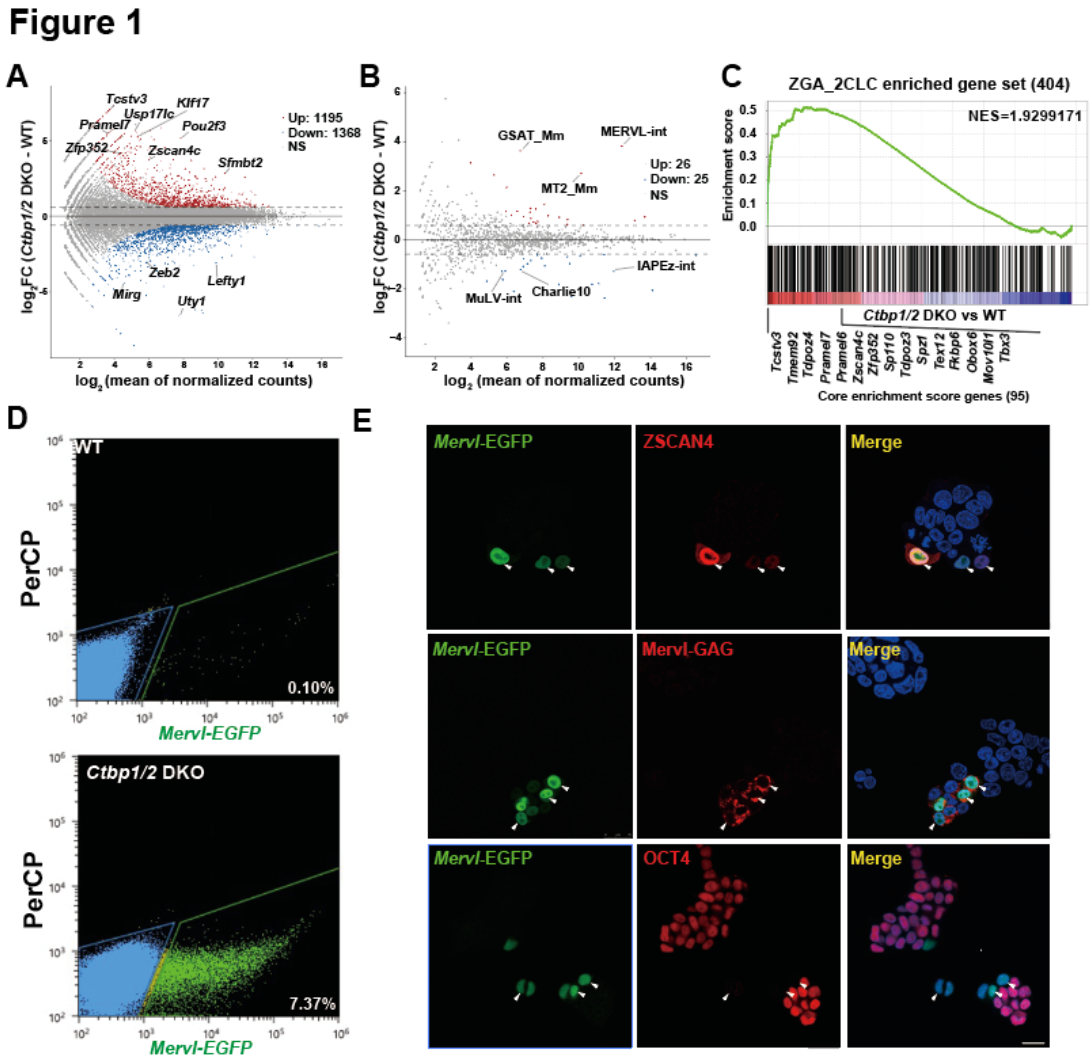

184

185 **Figure 1. Disruption of *Ctbp1/2* expands the 2-cell-like cell (2CLC) population.**

186 (A), (B) MA-plots showing the relationship between average gene (or repeat) expression

187 and $\log_2$ fold change between *Ctbp1/2* DKO and wild-type (WT) ESCs. Differentially

188 expression was defined as adjusted $p \leq 0.05$ and fold change ≥ 2. Red and blue dots

189 indicate up- and down-regulated genes, respectively. (C) Gene set enrichment analysis

190 (GSEA) of genes upregulated in 2-cell embryos compared with oocytes and enriched in

191 MERVL-positives 2CLCs relative to MERVL-negative ESCs (GSE33923) (Macfarlan et
192 al., 2012). (D) Flow cytometry analysis of MERVL::TurboGFP reporter activity in WT
193 ESCs and *Ctbp1/2* DKO ESCs. (E) Immunofluorescence analysis showing that
194 MERVL::TurboGFP-positive cells co-express ZSCAN4 and MERVL-GAG proteins, and
195 are mutually exclusive with OCT4 expression. Nuclei were counterstained with DAPI.
196 Scale bar: 10 μm.
197
198 ***CtBP1/2 repress DUX-dependent minor ZGA genes and DUX-independent maternal***
199 ***and major ZGA genes in ESCs***
200 DUX, the homeobox transcription factor, is both essential and sufficient for the
201 emergence of spontaneous 2CLCs from ESCs (De Iaco et al., 2017; Whiddon et al., 2017).
202 To determine whether the 2C-like program triggered by *Ctbp1/2* deficiency depends on
203 DUX, we deleted the *Dux* cluster in both WT and *Ctbp1/2* DKO ESCs (Supplementary
204 Figure 1C). We first compared the population of MERVL-EGFP-positive cells among
205 WT, *Dux* KO, *Ctbp1/2* DKO and *Ctbp1/2*/*Dux* triple-KO (TKO) ESCs. While the strong
206 GFP-positive population was markedly reduced in TKO compared to DKO ESCs, a weak
207 GFP-positive population persisted in the TKO (Figure 2A, B). RT-qPCR analysis
208 confirmed that *Pramel7*, which is upregulated at the 2C stage in WT and *Dux* KO
209 embryos (Guo et al., 2019), remained elevated in both DKO and TKO ESCs, indicating
210 DUX-independent activation (Figure 2C). In contrast, *Zscan4c* upregulation upon
211 *Ctbp1/2* depletion was completely abolished by *Dux* deletion, indicating strict DUX
212 dependency.

213 To assess transcriptional activity of the MERVL long terminal repeat (MERVL-LTR)
214 sequences, we performed a luciferase reporter assay (Supplemental Figure 2A). *Ctbp1/2*
215 loss led to robust activation of MERVL-LTR reporter, and mutation of DUX-binding
216 motif (DUXmut-MERVL-LTR) markedlyreduced, but did not abolish, this activity.
217 Reporter activity in *Ctbp1/2/Dux* TKO remained substantially higher than *Dux* KO,
218 indicating that CtBP1/2 also repress MERVL through DUX-independent mechanisms.
219 Published DUX ChIP-seq data (Hendrickson et al., 2017) revealed DUX occupancy near
220 both the *Zscan4c* and *Naalad2* loci, with strong binding signals overlapping MERVL-
221 LTR or MT2 family elements (Supplementary Figure 2B). At the *Zscan4c* locus, DUX
222 binds both proximal regulatory region with a strong peak and distal MERVL elements. At
223 the *Naalad2* locus, DUX-binding sites are exclusively overlapped with MERVL
224 sequences. Reporter assay confirmed that MERVL-independent elements proximal to the
225 *Zscan4c* locus were activated by *Ctbp1/2* loss in a DUX-dependent manner, whereas
226 MERVL-LTR-containing elements derived from the *Zscan4c* and *Naalad2* loci retained
227 partial activity even in *Ctbp1/2/Dux* TKO ESCs (Supplementary Figure 2C). These
228 luciferase assay results were consistent with our RNA-seq data (Supplementary Figure
229 2E).
230 We next performed RNA-seq to identify genes induced by *Ctbp1/2* loss that are DUX-
231 dependent or DUX-independent. A scatter plot comparing gene expression changes
232 between WT and *Ctbp1/2* DKO (Y-axis) and between *Ctbp1/2/Dux* TKO and *Dux* KO
233 (X-axis) revealed a moderate correlation (R = 0.52), suggesting that a substantial
234 population of CtBP1/2-regulated genes act independent of DUX (Figure 2D). Venn

235 diagram showed that more than 75% of genes upregulated in DKO were also upregulated
236 in TKO ESCs (Figure 2E).
237 To classify these regulatory patterns, we applied K-means clustering analysis (K=5) using
238 the 2,000 most variable genes across WT, *Dux* KO, *Ctbp1/2* DKO, and *Ctbp1/2/Dux* TKO
239 ESCs (Figure 2F, G). Cluster 1 genes (e.g., *Zscan4*, *Usp17*) were slightly repressed in
240 *Dux* KO ESCs but strongly upregulated in *Ctbp1/2* DKO ESCs, and this upregulation was
241 abolished by *Dux* KO, defining DUX-dependent minor ZGA genes. Cluster 2 genes (e.g.,
242 *Gadd45g*) were upregulated in both *Ctbp1/2* DKO and *Ctbp1/2/Dux* TKO ESCs,
243 representing DUX-independent target. Cluster 3 genes (e.g., *Gata1*, *Pramel7*, *Zscan5b*)
244 showed moderate downregulation in *Dux* KO ESCs and were modestly upregulated in
245 both *Ctbp1/2* DKO and *Ctbp1/2/Dux* TKO ESCs, corresponding to major ZGA and
246 maternal genes. Cluster 4 (e.g, *Spic*) genes were downregulated by *Dux* KO in WT ESCs.
247 However, this downregulation by *Dux* KO was not observed in *Ctbp1/2* DKO ESCs,
248 indicating that the loss of CtBP1/2 abolishes the dependency of these genes on DUX.
249 Cluster 5 genes were consistently downregulated in both *Ctbp1/2* DKO and *Ctbp1/2/Dux*
250 TKO ESCs, indicating positive regulation by CtBP1/2 in a DUX-independent manner.
251 To evaluate the expression dynamics of these clusters in early mouse embryos, we
252 compared these clusters with public RNA-seq data from early embyos (Zhang et al.,
253 2016), excluding genes with an FPKM average ≤ 1 (Figure 2H). Cluster 1 genes were
254 transient activated at the 2-4-cell stage, typical of minor ZGA genes, whereas Cluster2-4
255 included maternal genes downregulated post-fertilization and zygotic genes activated
256 after the late 2-cell stage.

257 Finally, to further examine the dependency of genes upregulated by *Ctbp1/2* DKO on
258 DUX, we measured the expression changes of genes belonging to Cluster 1 and 3 upon
259 inducible *Dux* expression using doxycycline-inducible *Dux* ESCs (Figure 2I). Consistent
260 with our RNA-seq data, Cluster 1 genes were consistently upregulated whereas Cluster 3
261 genes showed little or no change following short-term DUX induction. Taken together,
262 these results demonstrate that the *Ctbp1/2* depletion broadly upregulates DUX-dependent
263 minor ZGA genes and DUX-independent maternal and major ZGA genes, revealing a
264 dual regulatory system that links CtBP1/2-mediated repression to early embryonic
265 transcriptional programs.
266
267
268
269

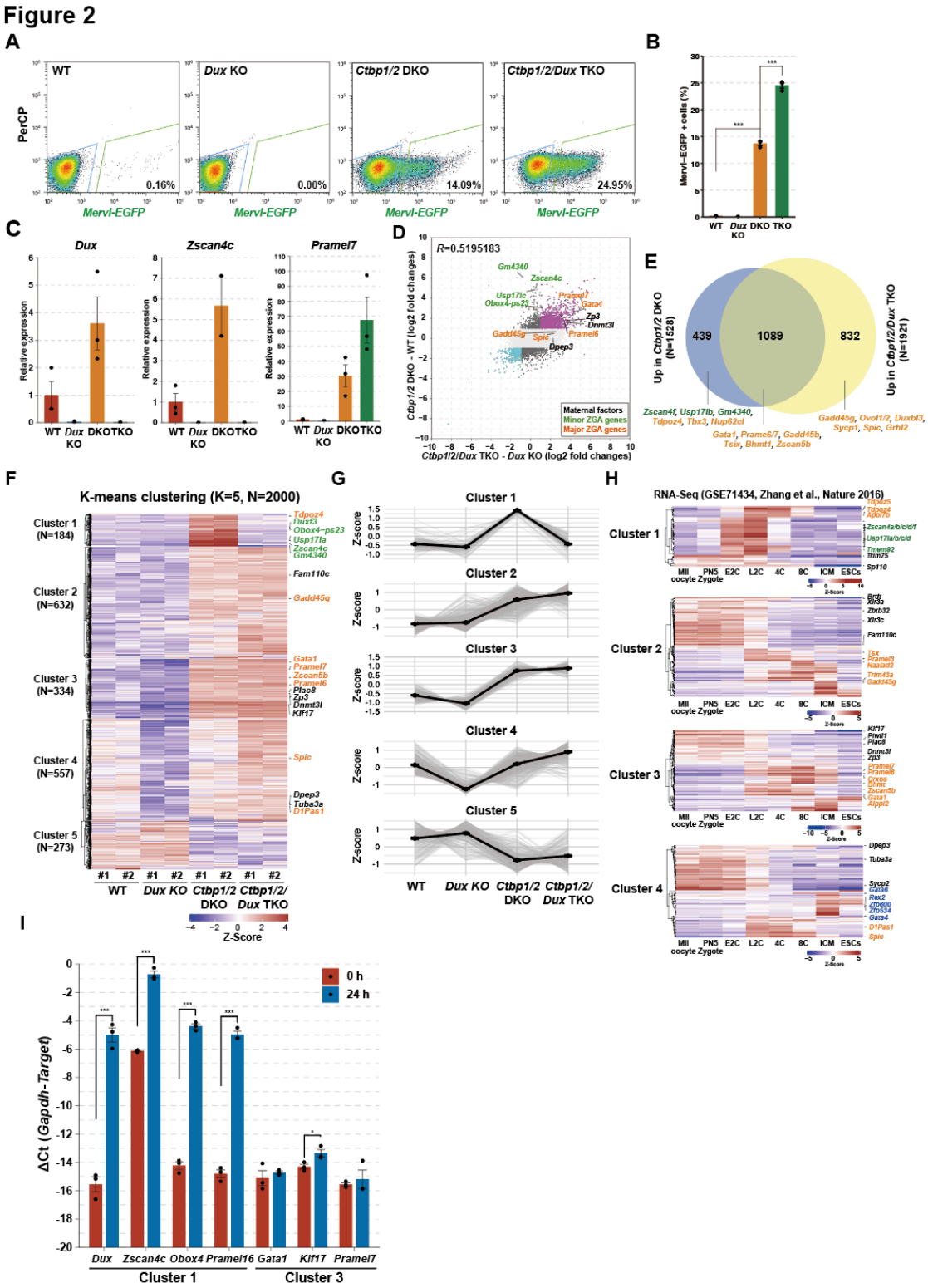

Figure 2. CtBP1/2 repress both DUX-dependent and -independent transcriptional programs associated with preimplantation embryos in mouse ESCs.

(A) Flow cytometry analysis (FACS) of MERVL::TurboGFP reporter expression in wild-

274 type (WT), *Dux* knockout (KO), *Ctbp1/2* double knockout (DKO) and *Ctbp1/2*/*Dux* triple
275 knockout (TKO) ESCs. (B) Percentage of MERVL-EGFP-positive cells obtained by
276 FACS Shown are standard error of means (SEM) at biological triplicates. (C) RT-qPCR
277 analysis of 2C-associated genes in WT, *Dux* KO, *Ctbp1/2* DKO and *Ctbp1/2*/*Dux* TKO
278 ESCs. Values are shown as relative expression with WT set to 1. Error bar indicates the
279 standard error of means. ***$P < 0.001$, **$P < 0.005$, *$P < 0.05$ (Tukey-Kramer multiple
280 comparison test). (D) Scatter plot comparing gene expression changes induced by
281 *Ctbp1/2* DKO in WT (Y-axis) and *Dux* KO (X-axis) backgrounds. (E) Venn diagram
282 showing the overlap of genes upregulated in *Ctbp1/2* DKO and TKO. (F) K-means
283 clustering analysis (K=5) of the top 2,000 differentially expressed genes across WT, *Dux*
284 KO, *Ctbp1/2* DKO and *Ctbp1/2/Dux* TKO ESCs. (G) Average expression profiles of
285 genes from each cluster at WT, *Dux* KO, *Ctbp1/2* DKO and *Ctbp1/2/Dux* TKO ESCs.
286 Grey lines indicate individual gene, and black line represents the average expression of
287 genes within each cluster. (H) Hierarchical clustering of genes from each cluster using
288 public RNA-seq data of early mouse embryo (Zhang et al., 2016). (I) RT-qPCR after *Dux*
289 induction (0 h vs 24 h) for selected genes (Cluster 1: *Dux, Zscan4c, Obox4, Pramel16*
290 *and Cluster 3: Gata1, Klf17, Pramel7*). The ΔCt of each gene was calculated by
291 subtracting the average Ct of Gapdh from that of each gene Ct. Means of ΔCt were
292 calculated from three biological triplicates. Error bar indicates the standard error of means
293 (SEM). ***$P < 0.001$, **$P < 0.005$, *$P < 0.05$ (Tukey-Kramer multiple comparison test).

294

295 ***Temporal regulation of ZGA-associated genes by CtBP1/2 defines rapid and delayed***
296 ***response genes***

297 To monitor the dynamics of ZGA-asscoated gene expression in response to CtBP2
298 induction and depletion in ESCs, we established *Ctbp1/2* DKO ESCs carrying a
299 doxycycline-inducible CtBP2 transgene. Using this system, we analyzed the expression
300 of representative ZGA-related genes by qRT-PCR. *Dux*, MERVL, *Zscan4c* and *Zfp352*
301 were markedly downregulated between day 3 and day 9 following CtBP2 induction, and

302 subsequently reactivated from day 12 to day 18 upon CtBP2 depletion (Figure 3A). In
303 contrast, *Pramel7* exhibited a rapid response, being strongly downregulated between
304 day 0 and day 3, and then upregulated between day 9 and day 12.
305 To distinguish between rapid and delayed transcriptional responses, we performed
306 RNA-seq using *Ctbp1/2* conditional KO (cKO) ESCs at defined time points. Principal
307 component analysis (PCA) revealed that short-term CtBP2 induction (days 0-3) and
308 depletion (days 9-12) drove opposing changes along the PC1 axis, whereas long-term
309 induction (days 3-9) and depletion (days 12-18) contributed to opposite shifts along
310 PC2 (Figure 3B). By overlapping differentially expressed genes under these conditions,
311 we identified two kinetically distinct groups: rapid-response genes, including major
312 ZGA genes (*Pramel7*, *Gata1*, *Phlda2*) and maternal factors (*Klf17*, *Pramel13*) (Figure
313 3C), and delayed-response genes, comprising minor ZGA genes such as *Zscan4*,
314 *Usp17l*, and *Gm4340* (Figure 3D). Temporal trajectory analysis showed that rapid-
315 response genes (N = 89) were immediately repressed upon CtBP2 induction (days 0-3)
316 and quickly reactivated following CtBP2 depletion (days 9-12) (Figure 3E). By
317 contrast, delayed-response genes (N = 48) displayed gradual downregulation during
318 CtBP2 expression and delayed recovery upon CtBP2 depletion (Figure 3F). Heatmap
319 analysis illustrated their distinct temporal expression patterns (Figure 3G).
320 Finally, to assess the DUX dependency of these gene sets, we compared gene
321 expression changes induced by *Ctbp1/2* DKO in WT and *Dux* KO backgrounds. Rapid-
322 response genes were equivalently upregulated in both context, whereas the induction of
323 delayed-response genes were significantly attenuated in the absence of DUX (Figure

3H). Collectively, these results indicate that CtBP1/2 represses two transcriptional cascades with distinct temporal kinetics: a DUX-independent program directly targeting major ZGA and maternal genes, and a DUX-dependent program that controls minor ZGA genes.

Figure 3

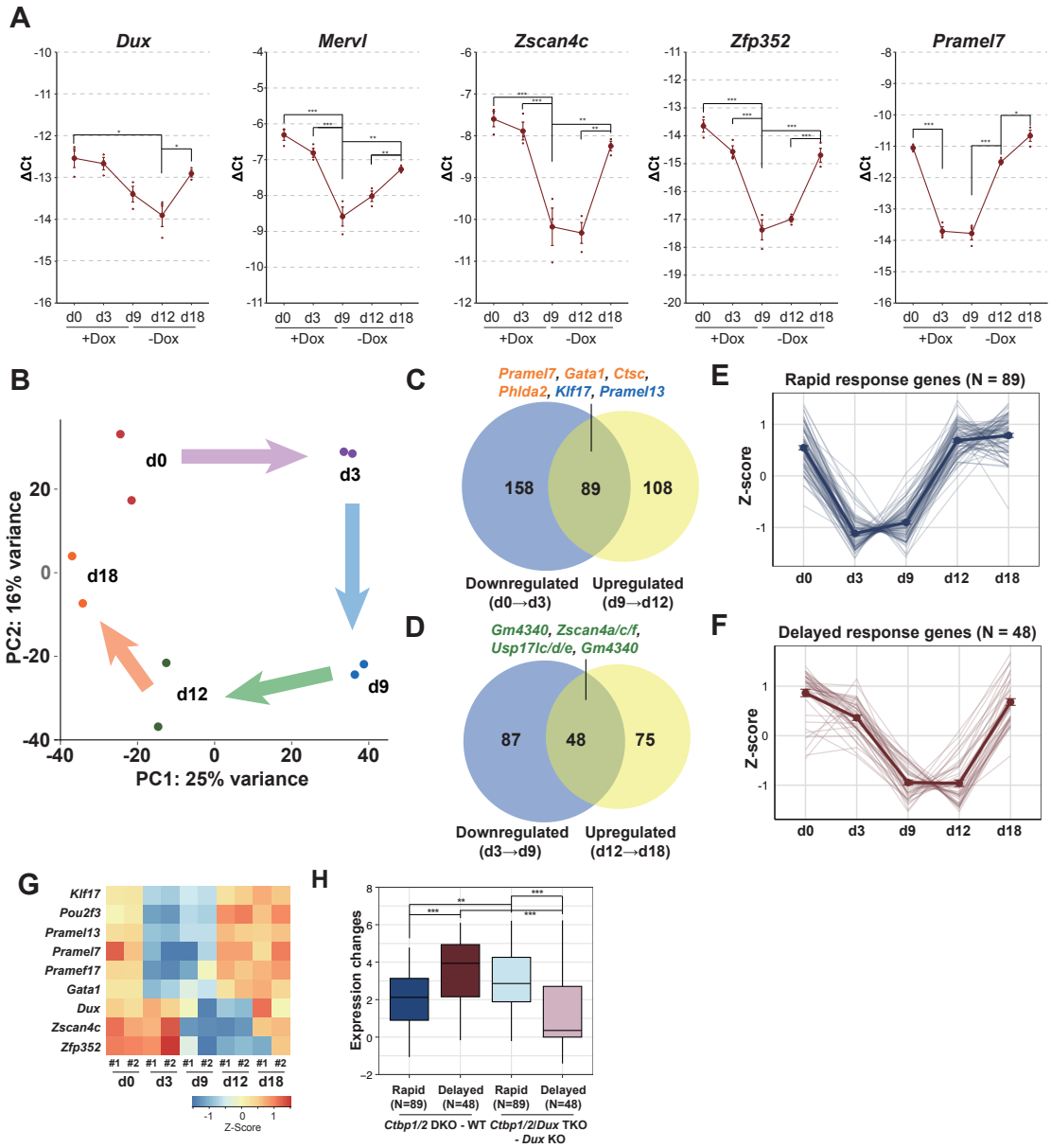

330 **Figure 3. Temporal regulation of ZGA genes by CtBP1/2 defines rapid and delayed**
331 **responses.**
332 (A) RT-qPCR analysis of *Dux*, MERVL*, Zscan4c Zfp352* and *Pramel7* in *Ctbp1/2* DKO
333 ESCs with or without doxycycline (Dox). The ΔCt of each gene was calculated by
334 subtracting the average Ct of *Gapdh* from that of each gene Ct. Means of ΔCt were
335 calculated from three biological triplicates. Error bars indicate the standard error of
336 means (SEM). ***$P < 0.001$, **$P < 0.005$, *$P < 0.05$ (Tukey-Kramer multiple
337 comparison test). (B) Principal component analysis (PCA) of *Ctbp1/2* DKO ESCs with
338 or without Dox. (C) Venn diagram showing the overlap between genes downregulated 3
339 days after CtBP2 induction and genes upregulated 3 days after CtBP2 depletion. (D)
340 Venn diagram showing the overlap between genes downregulated during CtBP2
341 induction (day3-9) and genes upregulated during CtBP2 depletion (day 12-18). (E, F)
342 Temporal expression dynamics of rapid and delayed response genes upon CtBP2
343 induction or depletion. Individual gene trajectories (thin lines) and the mean ± SEM
344 (bold lines with error bars) are shown for Rapid response genes (N = 89, panel E) and
345 Delayed response genes (N = 48, panel F). (G) Heatmap showing the expression
346 profiles of selected rapid and delayed response genes. (H) Boxplot showing expression
347 changes of rapid and delayed response genes upon CtBP1/2 depletion in wild-type and
348 *Dux* KO backgrounds.
349
350 ***CtBP2 directly represses major ZGA genes Pramel7 and Gata1 in ESCs***
351 To examine whether CtBP2 directly regulates major ZGA genes in ESCs, we analyzed
352 the CTBP2 occupancy at rapid- and delayed- response genes using public ChIP-seq
353 datasets (Kim et al., 2015). Genomic peaks were annotated to nearby genes using
354 Genomic Regions Enrichment of Annotations tools (GREAT) with the "two nearest
355 genes" setting (McLean et al., 2010), which assigns each regulatory region to the two
356 closest transcription start sites (TSSs) within 1 Mb (Figure 4A). Approximately half of
357 the rapid-response genes (40 out of 89), but only 2 of 48 delayed-response genes,

358 contained CtBP2-binding peaks. Genome browser views of H3K27Ac (Zhang et al.,
359 2020), a marker for active enhancers, DUX (Hendrickson et al., 2017), and CtBP2
360 occupancy demonstrated that CtBP2 was bound at regulatory regions of rapid-response
361 genes such as *Pramel7* and *Gata1*, whereas DUX binds to delayed-response loci such as
362 *Duxf3* and *Zscan4c* (Figure 4B, C).
363 To functionally validate the repressive activity of CtBP2-bound regions, we performed
364 luciferase reporter assays using distal enhancer fragments derived from *Pramel7* and
365 *Gata1* loci in wild-type and *Ctbp1/2* DKO ESCs. Each enhancer activities was elevated
366 in *Ctbp1/2* DKO ESCs and was suppressed upon CtBP2 re-expression (Figure 4D, E),
367 supporting the idea that CtBP2 directly represses *Gata1* and *Pramel7* transcription
368 through their distal enhancer elements in ESCs.
369 Immunofluorescence analysis further showed that MERVL-EGFP-positive cells
370 expressed GATA1 in WT ESCs, whereas this expression was abolished in *Dux* KO
371 ESCs (Figure 4F). Consistent with the FACS profiles described earlier (Figure 2A), we
372 observed both EGFP-weak and strong-populations in *Ctbp1/2* DKO ESCs, and both
373 populations expressed GATA1. Deletion of *Dux* in *Ctbp1/2* DKO ESCs abolished
374 selectively eliminated the EGFP-strong, and GATA1-positive cells, whereas the EGFP-
375 weak-positive cells, GATA1-positive cells persisted. These findings suggest that
376 *Ctbp1/2* DKO ESCs comprise two transcriptionally distinct 2CLC population: (1) a
377 DUX-dependent, GATA1-positive subset corresponding to classical 2CLCs marked by
378 strong MERVL-EGFP-strong expression, and (2) a DUX-independent, GATA1-positive
379 subset representing a novel 2CLC state associated with major ZGA gene activation.

380

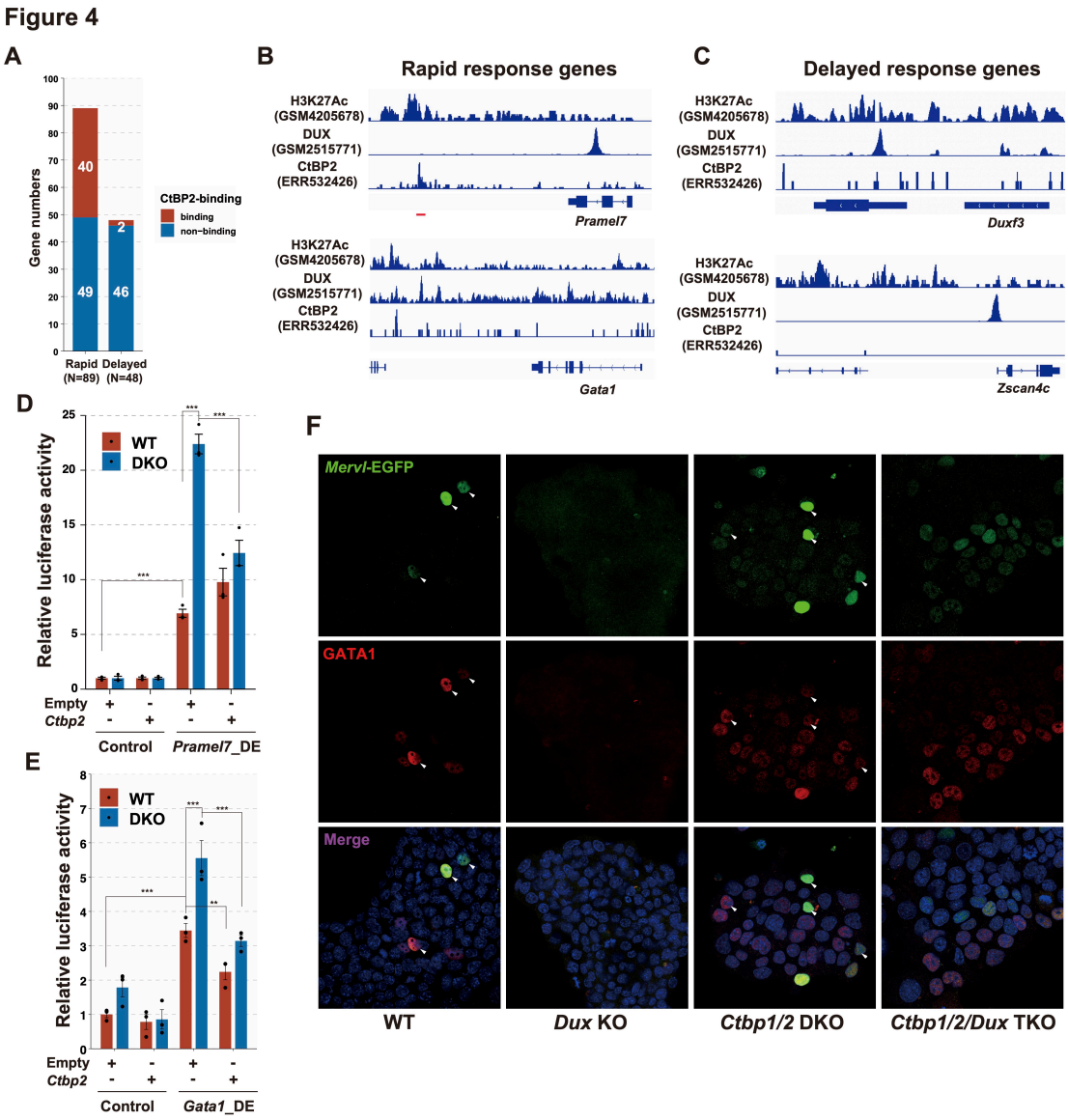

381

382 **Figure 4. Major ZGA genes, *Pramel7* and *Gata1*, are direct targets of CtBP2 in**

383 **ESCs.**

384 (A) Proportion of CtBP2-bound genes in rapid- and delayed-response groups based on
385 public CtBP2 ChIP-seq data (Kim et al., 2015). Peak-to-gene assignment performed
386 using GREAT (McLean et al., 2010) under the "two nearest genes" rule (≤1 Mb). (B, C)
387 Genome browser views showing H3K27ac (Zhang et al., 2020), DUX (Hendrickson et
388 al., 2017) and CtBP2 ChIP-seq signals at representative rapid (B) and delayed (C)

389 response genes. (D, E) Luciferase assays using distal regulatory regions of *Pramel7* (D)
390 or *Gata1* (E) loci in wild-type (WT) and *Ctbp1/2* DKO ESCs with or without CtBP2
391 overexpression. (F) Immunofluorescence analysis of WT, *Dux* KO, *Ctbp1/2* DKO and
392 *Ctbp1/2/Dux* TKO ESCs stained with anti-GFP (green) and GATA1 (red) antibodies.
393 Nuclei were counterstained with DAPI. Arrowheads indicate MERVL-EGFP-positive
394 cells.

395

396 ***PRAMEL7 regulates subsets of both DUX-dependent and -independent ZGA-***
397 ***associated genes***

398 *Pramel7* belongs to the PRAME (preferentially expressed antigen in melanoma) gene
399 family, whose expression is normally restricted to testis and cancers (Kern et al., 2021).
400 As the third largest gene family in mouse genome (Church et al., 2009), we examined
401 its regulation in wild-type (WT), *Dux* KO, *Ctbp1/2* DKO and *Ctbp1/2/Dux* TKO ESCs.
402 A phylogenetic tree constructed from amino acid sequences annotated in mm39
403 revealed that PRAME family genes are organized into six chromosomal clustres, with
404 high intracluster similarity (Supplementary Figure 3A, B). RNA-seq analysis showed
405 that most PRAME—except *Lrrc14*, *Lrrc14b*, and *Pramel48*—were markedly
406 upregulated in *Ctbp1/2* DKO ESCs (Figure 5A).
407 Based on expression patterns across WT, *Dux* KO, *Ctbp1/2* DKO and *Ctbp1/2/Dux*
408 TKO ESCs, PRAME genes were classified into four groups: (1) genes unaffected by
409 *Ctbp1/2* DKO (e.g., Lrrc14); (2) genes further upregulated by *Dux* KO (e.g.,
410 *Pramel14/30*); (3) genes suppressed by *Dux* KO (e.g., *Pramel16/19/31*, DUX-
411 dependent); and (4) genes unaffected by *Dux* KO (e.g., *Pramel7/12*, DUX-independent).
412 Single-cell RNA-seq analysis of early embryonic stages (Zhang et al., 2016) revealed

413 that DUX-dependent PRAME genes (e.g., *Pramel16/19/31*) are transiently induced at
414 the mid-2-cell stage. In contrast, DUX-independent PRAME genes could be further
415 subdivided into two categories (Figure 5B): (i) *Pramel6/7/30*, which are upregulated
416 from mid-2-cell and peak at ICM before being silenced in ESCs; and (ii) *Pramel12/13*,
417 which are maternally expressed and downregulated by at 4-cell stage.
418 Given the DUX-independent function of *Pramel7* and its known importance in early
419 mouse development (Graf et al., 2017), we generated ESCs overexpressing *Pramel7*
420 (P7OE) in both WT and *Dux* KO backgrounds (Figure 5C, D). *Pramel7* overexpression
421 increased the fraction of MERVL-EGFP-positive 2CLCs (Figure 5E, F), although to a
422 lesser extent than in *Ctbp1/2* DKO. This increase was abolished in *Dux* KO
423 background, and the MERVL-EGFP-weak positive population was absent, indicating
424 that PRAMEL7-driven 2CLC partially depends on DUX.
425 We next compared genes upregulated by PRAMEL7 with those upregulated by
426 *Ctbp/1/2* DKO in either DUX-dependent or -independent contexts. Venn diagram
427 analysis revealed that a subset of genes activated in a DUX-dependent (55 out of 390)
428 as well as DUX-independent manner (194 out of 1,097) upon *Ctbp1/2* DKO were also
429 upregulated by PRAMEL7 overexpression (Figure 5G). To further investigate the
430 transcriptional programs controlled by PRAMEL7, we performed K-means clustering
431 (K=5) of the top 1,000 most variable genes from RNA-seq of WT, *Dux* KO, P7OE and
432 P7OE/*Dux* KO ESCs (Figure 5H). Cluster 1 contained PRAMEL7-induced genes
433 unaffected by *Dux* KO, including germline-specific and DNA methylation-repressed
434 genes (e.g., *Xlr3/4/5*, *Hormad1*) (Escalier et al., 2002; Shin et al., 2010), which were

435 enriched for meiotic cell cycle pathways (Figure 5I). Cluster 3 genes, including *Zscan4*
436 and *Usp17l* family members, were upregulated by PRAMEL7 overexpression but
437 completely abolished upon *Dux* KO background (Figure 5J), indicating that PRAMEL7
438 indirectly promotes the expression of minor ZGA genes through *Dux* activation,
439 consistent with increased *Duxf3* expression (Figure 5J). Cluster 4 comprised genes
440 downregulated by *Dux* KO ESCs in WT ESCs but not in P7OE ESCs, suggesting that
441 these genes are suppressed as a consequence of *Pramel7* downregulation in the absence
442 of DUX. Consistent with this, *Pramel7* expression was significantly reduced in Dux KO
443 ESCs (Figure 5K). Together, these results identify PRAMEL7 as a key mediator that
444 links DUX-dependent and -independent transcriptional programs in establishing the
445 totipotent-like states.
446

Figure 5

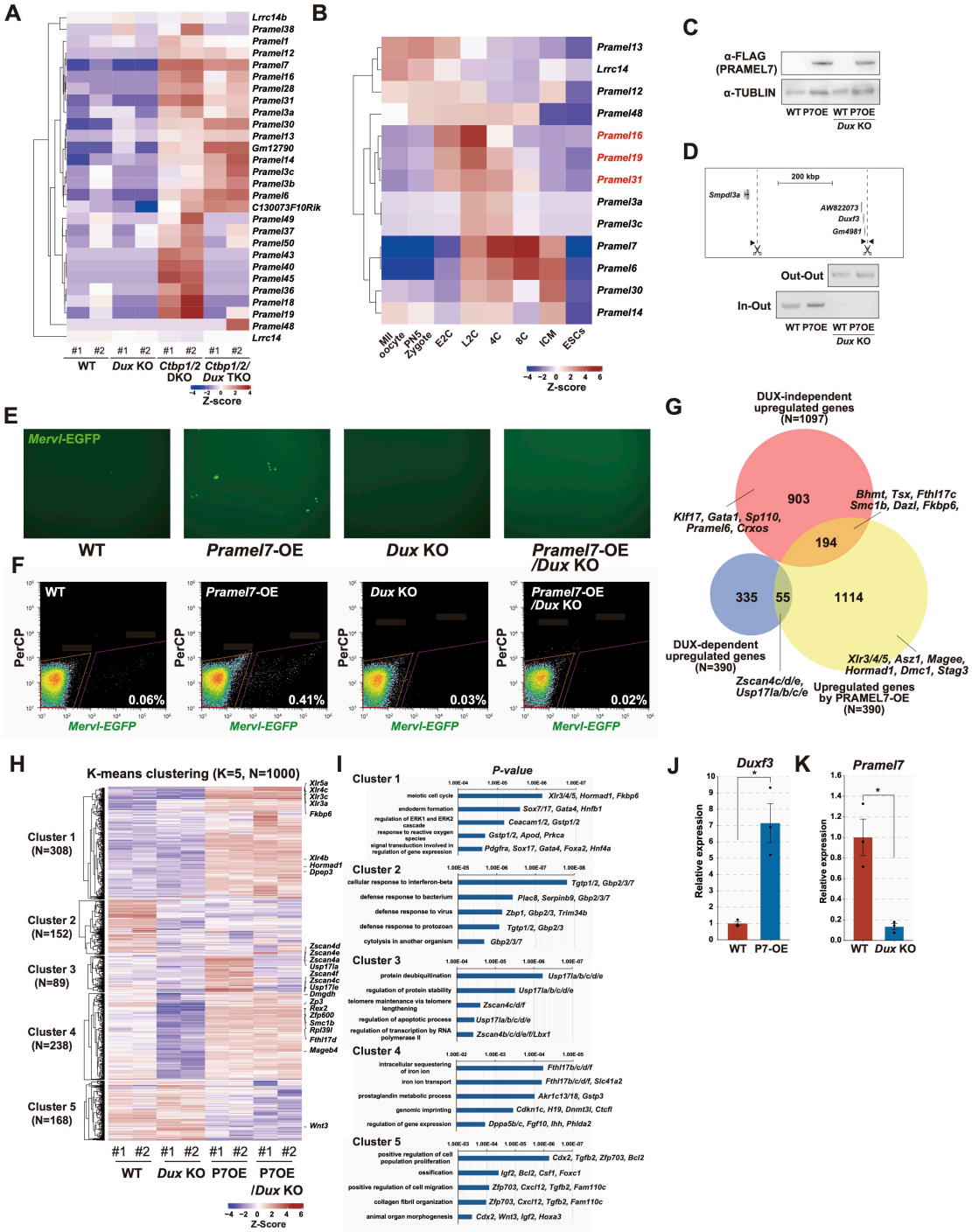

447

448

449 **Figure 5. PRAMEL7 controls a subset of ZGA-associated genes through DUX-**

450 **dependent and -independent mechanisms.**

451 (A) Hierarchical clustering heatmap of of PRAME family genes from RNA-seq of wild-
452 type (WT), *Dux* KO, *Ctbp1/2* DKO and *Ctbp1/2*/*Dux* KO ESCs. (B) Expression dynamics
453 of PRAME family genes during early mouse embryos (Zhang et al., 2016). Red letters
454 indicate DUX-dependent genes. (C) Western blot analysis of FLAG-tagged PRAMEL7
455 protein levels WT, PRAMEL7-overexpressing (P7OE), *Dux* KO and P7OE/*Dux* KOESCs.
456 (D) Genotype PCR confirming large deletion of *Dux* cluster locus using primer sets
457 flanking the gRNA target site. (E) Fluorescence images showing MERVL-EGFP signals
458 in WT, P7OE, *Dux* KO and P7OE/*Dux* KO ESCs. (F) FACS analysis quantifying the
459 percentage of MERVL-EGFP-positive cells in WT, P7OE, *Dux* KO and P7OE/*Dux* KO
460 ESCs. (G) Venn diagram showing the overlap of genes upregulated by *Ctbp1/2* DKO
461 (with or without DUX) and those induced by PRAMEL7 overexpression (H) K-means
462 clustering (K=5) of the top 1,000 most variable genes from RNA-seq of WT, P7OE, *Dux*
463 KO and P7OE/*Dux* KO ESCs. ((I) Gen ontology enrichment analysis of each gene cluster
464 identified in (H). (J) RT-qPCR analysis of *Duxf3* in WT and P7OE ESCs. (K) RT-qPCR
465 analysis of *Pramel7* in WT and <u>*Dux*</u> KO ESCs. The ΔCt values were calculated relative
466 to *Gapdh*, and error bar indicates the standard error of means (SEM) from three biological
467 replicates. Statistical significance was assessed by Tukey-Kramer multiple comparison
468 test (***$P < 0.001$, **$P < 0.005$, *$P < 0.05$).

469

470 ***Dux controls part of the ZGA transcriptional program through PRAMEL7 functions***

471 To investigate the functional relationship between DUX and PRAMEL7, we generated
472 *Pramel7* KO ESCs and compared transcriptomic changes between *Dux* KO and
473 *Pramel7* KO ESCs using scatter plot analysis (Figure 6A). Global expression alterations
474 showed a moderate positive correlation ($R = 0.39$), particularly among downregulated
475 genes. Gene ontology (GO) analysis of genes downregulated in both *Pramel7* KO and
476 *Dux* KO ESCs revealed enrichment for terms related to "Nucleic acid binding" and
477 "Homeodomain", including *Zfp600*, *Zic2* and *Cphx*, *Pou3f1*. In contrast, genes
478 downregulated genes only in *Dux* KO were enriched for "Multicellular organism

479 development" and "Metal ion binding", including *Piwil1*, *Dppa5* and *Zsacn4c*, *Gata1/2*
480 (Figure 6B). The Overlap between genes upregulated in *Dux* KO and *Pramel7* KO was
481 modest compared with strong overlap observed for downregulated genes (Figure 6C).
482 Furthermore, GSEA demonstrated that the overexpression of PRAMEL7 in *Dux* KO
483 ESCs effectively rescued the downregulated genes resulting from *Dux* KO (Figure 6D),
484 indicating that downregulation of *Pramel7* expression is major cause of the
485 transcriptional abnormalities in *Dux* KO ESCs.
486 Because PRAMEL7 is known to promote UHRF1 degradation, we next examined
487 whether DNA methylation contributes to gene silencing in *Dux* and *Pramel7* KO ESCs.
488 More than half of the genes downregulated in both *Dux* KO and *Pramel7* ESCs were
489 upregulated by *Dnmt1* KO ESCs (Figure 6E), suggesting that the transcriptional
490 repression observed in these mutants is mediated, at least in part, by aberrant DNA
491 methylation.
492 We next analyzed the expression dynamics of genes downregulated in both *Dux* KO and
493 *Pramel7* KO ESCs, as well as those specifically downregulated only in *Dux* KO ESCs,
494 using public single-cell RNA-seq data from early mouse embryos (Zhang et al., 2016).
495 Gene downregulated genes both in *Dux* KO and *Pramel7* KO ESCs were primarily
496 associated with maternally expressed genes, major ZGA genes and post-ZGA genes
497 (Figure 6F). In contrast, genes downregulated only in *Dux* KO ESCs included not only
498 maternally expressed genes, major ZGA genes and post-ZGA genes but also minor
499 ZGA genes (Figure 6G).

Taken together, these findings suggest a mechanistic model in which DUX primarily activate minor ZGA genes, whereas PRAMEL7—one of the indirect downstream targets of DUX—regulates maternally, major ZGA genes and post-ZGA genes through modulation of DNA methylation mediated by UHRF1 degradation in 2CLCs.

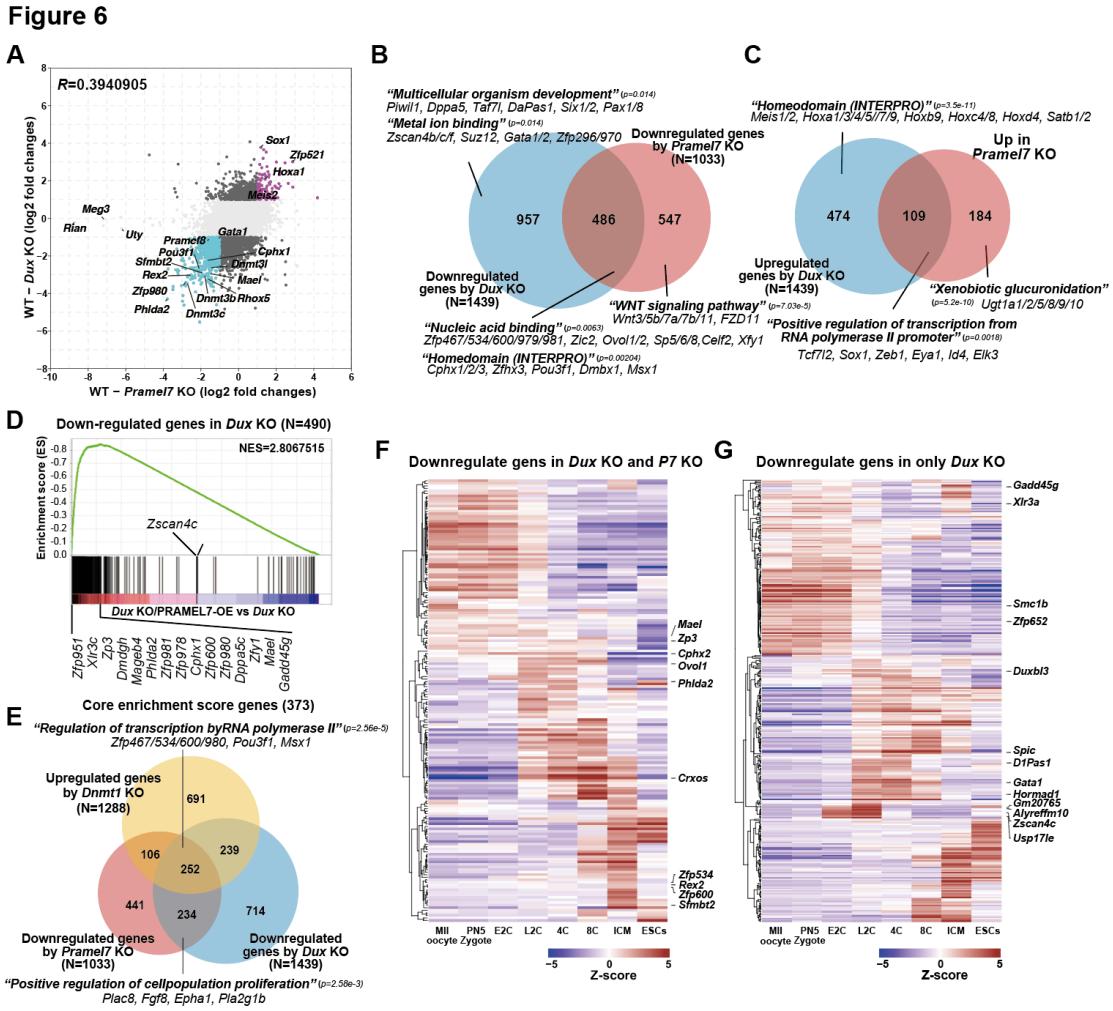

Figure 6. DUX regulates part of ZGA gene program through activation or *Pramel7* in ESCs.

(A) Scatter plot showing the correlation between expression changes in *Dux* KO and *Pramel7* KO ESCs. (B) Venn diagram showing the overlapping of the downregulated

genes by *Dux* KO in ESCs with the downregulated genes by *Pramel7* KO in ESCs. (C) Venn diagram showing the overlapping of the upregulated genes by *Dux* KO in ESCs with the upregulated genes by *Pramel7* KO in ESCs. (D) Gene set enrichment analysis (GSEA) using genes downregulated by the *Dux* KO to compare gene expression between PRMAEL7-overexpressing in *Dux* KO ESCs and *Dux* KO ESCs. (E) Venn diagram showing the overlap among genes upregulated in *Dnmt1* KO ESCs and genes downregulated in *Pramel7* KO and *Dux* KO ESCs. (F, G) Heatmaps showing hierarchical clustering of genes downregulated genes in both *Dux* KO and *Pramel7* KO ESCs (F), or exclusively in *Dux* KO ESCs (G), using public RNA-seq data of early mouse embryo (Zhang et al., 2016).

522 **Discussion**

523

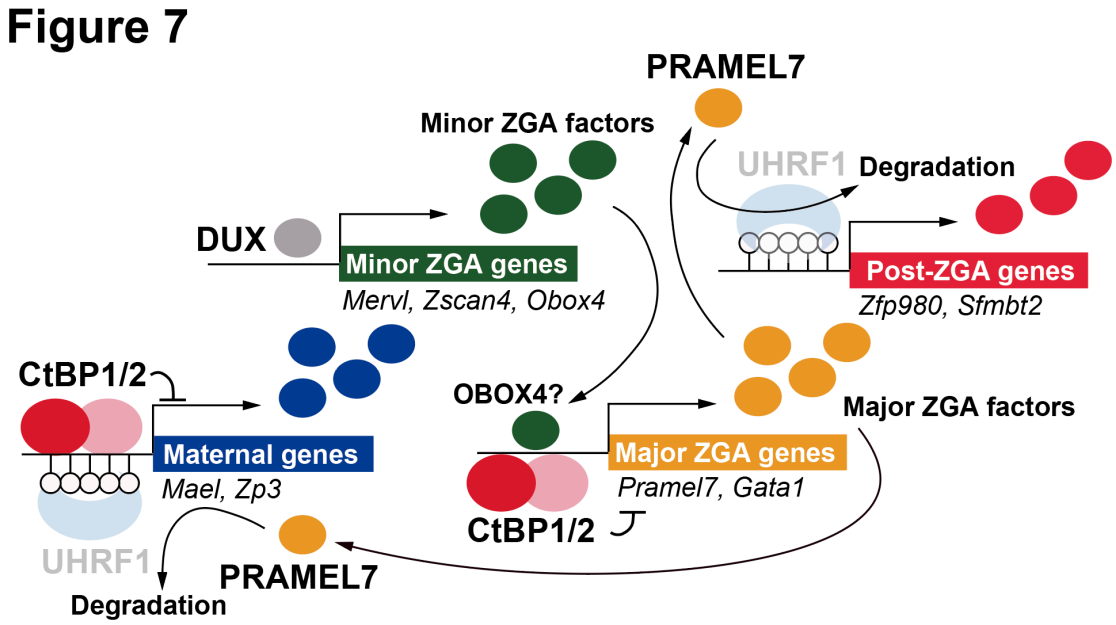

524

525 **Figure 7. A schematic model for the regulation of 2C-related genes by DUX, CtBP1/2**

526 **and PRAMEL7.**

527

528 In this study, we demonstrate that the loss of *Ctbp1/2* in ESCs activates both DUX-

529 dependent and DUX-independent transcriptional cascades to establish a totipotent-like

530 state (Figure 7). Most DUX-dependent genes activated upon *Ctbp1/2* depletion

531 correspond to minor ZGA genes transiently expressed at the two-cell (2C) stage. In

532 contrast, DUX-independent genes upregulated upon *Ctbp1/2* loss can be classified into

533 maternally expressed genes and post-major ZGA genes. Among them, *Pramel7* is directly

534 upregulated by *Ctbp1/2* loss in a DUX-independent manner and further modulates both

535 DUX-dependent and -independent pathways through the activation of DUX and its

536 downstream targets. Collectively, these findings uncover a dual regulatory framework in

537 which CtBP1/2 represses both DUX-mediated and DUX-independent transcriptional
538 programs, providing new insights into molecular mechanisms governing early mouse
539 embryogenesis.

540 Our data clearly demonstrate that the loss of *Ctbp1/2* in ESCs upregulates maternally
541 expressed and post-major ZGA genes in a DUX-independent manner, highlighting an
542 alternative regulatory axis operating during early embryonic development. Interestingly,
543 recent studies have demonstrated that OBOX proteins, a family of PRD-like homeobox
544 transcription factors, can compensate for DUX function by directly activating MERVL as
545 well as both minor and major ZGA genes (Guo et al., 2024; Ji et al., 2023; Sakamoto et
546 al., 2024). However, our transcriptome analysis revealed that only *Obox4* was upregulated
547 in *Ctbp1/2* double-knockout (DKO) ESCs, and this upregulation was completely
548 abolished by *Dux* KO. These results suggest that the loss of *Ctbp1/2* regulates early
549 developmental genes through pathways independent of both DUX and OBOX.

550 By integrating transcriptome data from conditional *Ctbp2* KO ESCs with public CtBP2
551 ChIP-seq datasets, we identified direct CtBP2 target genes (e.g., *Pramel7*, *Gata1*, and
552 *Klf17*) and distinguished them from DUX-dependent regulatory genes. Furthermore, we
553 found that MERVL-EGFP-weak positive cells in both *Ctbp1/2* DKO and *Ctbp1/2/Dux*
554 TKO ESCs expressed GATA1, a direct CtBP2 target. Importantly, GATA1-positive cells
555 were absent in *Dux* KO ESCs, suggesting that *Ctbp1/2* loss not only relieves DUX
556 dependency but also rewires the transcriptional hierarchy governing ZGA-associated
557 programs.

558 *Prame* is one of the most amplified gene families in mammals, and the mouse *Prame*

559 gene family represents the third-largest multigene family in the genome (Chang et al.,
560 2011). We showed that the disruption of *Ctbp1/2* activates the majority of *Prame* family
561 genes in ESCs, some of which are upregulated by DUX, while others are induced directly
562 by the loss of CtBP1/2. DUX-dependent *Prame* genes are enriched among minor ZGA
563 genes, whereas DUX-independent *Prame* genes are upregulated after major ZGA.
564 Moreover, many *Prame* genes are rapidly repressed upon the re-expression of CtBP2 in
565 *Ctbp1/2* DKO ESCs, indicating direct repression by CtBP1/2.
566 The positive regulators of *Prame* family genes remain largely unknown. Notably,
567 published RNA-seq data indicate that OBOX3/5, but not DUX, can activate *Pramel7* and
568 *Pramef17* (*Pramel14*), both of which are upregulated by *Ctbp1/2* loss even in the absence
569 of DUX. In contrast, *Pramel16*, *Gm12794* (*Pramel19*) and *A430089l19Rik* (*Pramel39*)
570 require DUX for activation (Sakamoto et al., 2024). Because *Obox* family genes were
571 silenced in *Ctbp1/2/Dux* TKO ESCs, it is possible that another positive regulator, distinct
572 from OBOX proteins, is activated upon *Ctbp1/2* depletion or constitutively expressed in
573 WT ESCs. Expression of *Prame* family genes has been observed in various cancer and
574 germline cells (Kern et al., 2021), and their expression pattern resembles that of *Pou5f1*
575 (Oct4) (Bortvin et al., 2003), suggesting that an OCT4-centered transcriptional network
576 may function as a positive regulatory axis for *Prame* genes.
577 We further demonstrated that the overexpression of PRAMEL7 partially rescues the
578 transcriptional abnormalities observed in *Dux* KO ESCs, in which *Pramel7* expression
579 was markedly reduced. PRAMEL7 activates two distinct genetic programs: one involving
580 minor ZGA genes through *Dux* upregulation, and another encompassing maternally

581 expressed, major ZGA and post-ZGA genes. Previous work showed that PRAMEL7
582 promotes global DNA demethylation by targeting UHRF1 for proteasomal degradation
583 in ESCs (Graf et al., 2017). In addition, *Dux* expression is epigenetically repressed by
584 DNA methylation maintained by the ZBTB24-CDCA7-HELLS axis (Guo et al., 2025).
585 These findings suggest that PRAMEL7 regulates DUX-dependent transcriptional
586 cascades by promoting DNA demethylation at the *Dux* locus. Furthermore, we found that
587 maternally expressed and major ZGA genes regulated by PRAMEL7 are also activated
588 upon *Dnmt1* depletion, indicating that PRAMEL7 controls these genes through DNA
589 demethylation mediated by UHRF1 degradation. Because PRAMEL7 also promotes
590 degradation of NuRD complex at chromatin to sustain pluripotency in ESCs (Rupasinghe
591 et al., 2024), it will be important to explore whether NuRD degradation by PRAMEL7
592 contributes to the regulation of ZGA-associated transcriptional programs.
593 Although DUX is a master regulator of the transition from pluripotent ESCs to 2-cell-like
594 cells, our results demonstrated that PRAMEL7 overexpression rescues most of the defects
595 observed in *Dux* KO ESCs. *Prame* family genes are upregulated from the early phase of
596 2CLC emergence traced by the *Zscan4* and MERVL reporter system based on scRNA-
597 seq (Eckersley-Maslin et al., 2016; Rodriguez-Terrones et al., 2018), and MERVL-
598 positive 2CLCs are eliminated by *Dux* KO (De Iaco et al., 2017). Our data further showed
599 that *Pramel7* expression was significantly reduced upon *Dux* KO in WT ESCs but
600 remained unaffected in *Ctbp1/2* DKO ESCs, indicating that the loss of *Ctbp1/2* rescues
601 the *Dux* KO phenotypic consequences through *Pramel7* upregulation in ESCs. Taken
602 together, we propose that DUX orchestrates two distinct transcriptional programs in early

603 mouse embryos: (1) direct activation of minor ZGA genes (e.g., MERVL, *Zscan4c* and
604 *Obox4*), and (2) PRAMEL7-mediated transcriptional cascades. While *Dux* KO ESCs
605 exhibit a marked reduction in *Pramel7* expression, *Pramel7* remains normally expressed
606 in *Dux* KO embryos at the mid-2C stage (Guo et al., 2019). OBOX5, which is maternally
607 expressed, represents a strong candidate regulator for the DUX-independent activation of
608 *Pramel7* in *Dux* KO embryos.
609 Our findings highlight fundamental differences between *in vitro* induction of 2CLCs and
610 *in vivo* regulation of ZGA, which are likely governed by maternal factors such as OBOX
611 and CtBP2. To better characterize these DUX-independent cascades, dual-reporter ESC
612 models (e.g., MERVL-tdTomato/*Gata1* or *Pramel7*-EGFP reporters) combined with
613 single-cell RNA-seq represent powerful approaches to dissect the molecular networks
614 underlying 2CLC heterogeneity induced by *Ctbp/1/2* loss.
615

References

Bortvin, A., Eggan, K., Skaletsky, H., Akutsu, H., Berry, D. L., Yanagimachi, R., Page, D. C. and Jaenisch, R. (2003). Incomplete reactivation of Oct4-related genes in mouse embryos cloned from somatic nuclei. *Development* **130**, 1673–1680.

Chang, T. C., Yang, Y., Yasue, H., Bharti, A. K., Retzel, E. F. and Liu, W. S. (2011). The expansion of the PRAME gene family in Eutheria. *PLoS One* **6**,.

Chen, Z. and Zhang, Y. (2019). Loss of DUX causes minor defects in zygotic genome activation and is compatible with mouse development. *Nat Genet* **51**, 947–951.

De Iaco, A., Planet, E., Coluccio, A., Verp, S., Duc, J. and Trono, D. (2017). DUX-family transcription factors regulate zygotic genome activation in placental mammals. *Nat Genet* **49**, 941–945.

Eckersley-Maslin, M. A., Svensson, V., Krueger, C., Stubbs, T. M., Giehr, P., Krueger, F., Miragaia, R. J., Kyriakopoulos, C., Berrens, R. V., Milagre, I., et al. (2016). MERVL/Zscan4 Network Activation Results in Transient Genome-wide DNA Demethylation of mESCs. *Cell Rep* **17**, 179–192.

Eckersley-maslin, M. A., Alda-catalinas, C. and Reik, W. (2018). Dynamics of the epigenetic landscape during the maternal- to-zygotic transition. *Nat Rev Mol Cell Biol* **19**, 436–450.

Eckersley-Maslin, M., Alda-Catalinas, C., Blotenburg, M., Kreibich, E., Krueger, C. and Reik, W. (2019). Dppa2 and Dppa4 directly regulate the Dux-driven zygotic transcriptional program. *Genes Dev* **33**, 194–208.

Escalier, D., Eloy, L. and Garchon, H. J. (2002). Sex-specific gene expression during meiotic prophase I: Xlr (X linked, lymphocyte regulated), not its male homologue Xmr (Xlr related, meiosis regulated), is expressed in mouse oocytes. *Biol Reprod* **67**, 1646–1652.

Ge, S. X., Son, E. W. and Yao, R. (2018). iDEP: An integrated web application for differential expression and pathway analysis of RNA-Seq data. *BMC Bioinformatics* **19**, 1–24.

Graf, U., Casanova, E. A., Wyck, S., Dalcher, D., Gatti, M., Vollenweider, E., Okoniewski, M. J., Weber, F. A., Patel, S. S., Schmid, M. W., et al. (2017). Pramel7 mediates ground-state pluripotency through proteasomal-epigenetic combined pathways. *Nat Cell Biol* **19**, 763–773.

648 **Grow, E. J., Weaver, B. D., Smith, C. M., Guo, J., Stein, P., Shadle, S. C.,**
649 **Hendrickson, P. G., Johnson, N. E., Butterfield, R. J., Menafra, R., et al.** (2021).
650 p53 convergently activates Dux/DUX4 in embryonic stem cells and in
651 facioscapulohumeral muscular dystrophy cell models. *Nat Genet* **53**, 1207–1220.
652 **Guo, M., Zhang, Y., Zhou, J., Bi, Y., Xu, J., Xu, C., Kou, X., Zhao, Y., Li, Y., Tu, Z.,**
653 **et al.** (2019). Precise temporal regulation of Dux is important for embryo
654 development. *Cell Res* **7**, 1–4.
655 **Guo, Y., Kitano, T., Inoue, K., Murano, K., Hirose, M., Li, T. D., Sakashita, A., Ishizu,**
656 **H., Ogonuki, N., Matoba, S., et al.** (2024). Obox4 promotes zygotic genome
657 activation upon loss of dux. *Elife* **13**, 1–25.
658 **Guo, D., Du, Z., Liu, Y., Lin, M., Lu, Y., Hardikar, S., Xue, Y., Zhang, J., Chen, T.**
659 **and Dan, J.** (2025). The ZBTB24-CDCA7-HELLS axis suppresses the totipotent
660 2C-like reprogramming by maintaining Dux methylation and repression. *Nucleic*
661 *Acids Res* **53**,.
662 **Hendrickson, P. G., Doráis, J. A., Grow, E. J., Whiddon, J. L., Lim, J.-W., Wike, C.**
663 **L., Weaver, B. D., Pflueger, C., Emery, B. R., Wilcox, A. L., et al.** (2017).
664 Conserved roles of mouse DUX and human DUX4 in activating cleavage-stage
665 genes and MERVL/HERVL retrotransposons. *Nat Genet* **49**, 925–934.
666 **Hu, Z., Tan, D. E. K., Chia, G., Tan, H., Leong, H. F., Chen, B. J., Lau, M. S., Tan,**
667 **K. Y. S., Bi, X., Yang, D., et al.** (2020). Maternal factor NELFA drives a 2C-like
668 state in mouse embryonic stem cells. *Nat Cell Biol* **22**, 175–186.
669 **Hulsen, T., de Vlieg, J. and Alkema, W.** (2008). BioVenn - A web application for the
670 comparison and visualization of biological lists using area-proportional Venn
671 diagrams. *BMC Genomics* **9**, 1–6.
672 **Ishiuchi, T., Enriquez-Gasca, R., Mizutani, E., Bošković, A., Ziegler-Birling, C.,**
673 **Rodriguez-Terrones, D., Wakayama, T., Vaquerizas, J. M. and Torres-Padilla,**
674 **M.-E.** (2015). Early embryonic-like cells are induced by downregulating
675 replication-dependent chromatin assembly. *Nat Struct Mol Biol* **22**, 662–71.
676 **Ji, S., Chen, F., Stein, P., Wang, J., Zhou, Z., Wang, L., Zhao, Q., Lin, Z., Liu, B., Xu,**
677 **K., et al.** (2023). OBOX regulates mouse zygotic genome activation and early
678 development. *Nature* **620**, 1047–1053.
679 **Kern, C. H., Yang, M. and Liu, W. S.** (2021). The PRAME family of cancer testis
680 antigens is essential for germline development and gametogenesis. *Biol Reprod* **105**,

290–304.

Kim, T. W., Kang, B. H., Jang, H., Kwak, S., Shin, J., Kim, H., Lee, S. E., Lee, S. M., Lee, J. H., Kim, J. H., et al. (2015). Ctbp2 Modulates NuRD-Mediated Deacetylation of H3K27 and Facilitates PRC2-Mediated H3K27me3 in Active Embryonic Stem Cell Genes during Exit from Pluripotency. *Stem Cells* **33**, 2442–2455.

Kreibich, E., Blotenburg, M., Alda-Catalinas, C., Reik, W., Krueger, C. and Eckersley-Maslin, M. (2019). Dppa2 and Dppa4 directly regulate the Dux-driven zygotic transcriptional program. *Genes Dev* **33**, 194–208.

Macfarlan, T. S., Gifford, W. D., Driscoll, S., Lettieri, K., Rowe, H. M., Bonanomi, D., Firth, A., Singer, O., Trono, D. and Pfaff, S. L. (2012). Embryonic stem cell potency fluctuates with endogenous retrovirus activity. *Nature* **487**, 57–63.

McLean, C. Y., Bristor, D., Hiller, M., Clarke, S. L., Schaar, B. T., Lowe, C. B., Wenger, A. M. and Bejerano, G. (2010). GREAT improves functional interpretation of cis-regulatory regions. *Nat Biotechnol* **28**, 495–501.

Percharde, M., Lin, C., Yin, Y., Huang, B., Shen, X., Ramalho-santos, M., Percharde, M., Lin, C., Yin, Y., Guan, J., et al. (2018). Article A LINE1-Nucleolin Partnership Regulates Early Development and ESC Identity Article A LINE1-Nucleolin Partnership Regulates Early Development and ESC Identity. *Cell* **174**, 1–15.

Rodriguez-Terrones, D., Gaume, X., Ishiuchi, T., Weiss, A., Kopp, A., Kruse, K., Penning, A., Vaquerizas, J. M., Brino, L. and Torres-Padilla, M. E. (2018). A molecular roadmap for the emergence of early-embryonic-like cells in culture. *Nat Genet* **50**, 106–119.

Rupasinghe, M., Bersaglieri, C., Leslie Pedrioli, D. M., Pedrioli, P. G. A., Panatta, M., Hottiger, M. O., Cinelli, P. and Santoro, R. (2024). PRAMEL7 and CUL2 decrease NuRD stability to establish ground-state pluripotency. *EMBO Rep* **25**, 1453–1468.

Sakamoto, M., Ito, A., Wakayama, S., Sasaki, H., Wakayama, T. and Ishiuchi, T. (2024). Detection of newly synthesized RNA reveals transcriptional reprogramming during ZGA and a role of Obox3 in totipotency acquisition. *Cell Rep* **43**, 114118.

Shin, Y. H., Choi, Y., Erdin, S. U., Yatsenko, S. A., Kloc, M., Yang, F., Wang, P. J., Meistrich, M. L. and Rajkovic, A. (2010). Hormad1 mutation disrupts synaptonemal complex formation, recombination, and chromosome segregation in

714 mammalian meiosis. *PLoS Genet* **6**,.
715 **Stankiewicz, T. R., Gray, J. J., Winter, A. N. and Linseman, D. A.** (2014). C-terminal
716 binding proteins: Central players in development and disease. *Biomol Concepts* **5**,
717 489–511.
718 **Whiddon, J. L., Langford, A. T., Wong, C. J., Zhong, J. W. and Tapscott, S. J.** (2017).
719 Conservation and innovation in the DUX4-family gene network. *Nat Genet* **49**, 935–
720 940.
721 **Wu, K., Liu, H., Wang, Y., He, J., Xu, S., Chen, Y., Kuang, J., Liu, J., Guo, L., Li, D.,**
722 **et al.** (2020). SETDB1-Mediated Cell Fate Transition between 2C-Like and
723 Pluripotent States. *Cell Rep* **30**, 25-36.e6.
724 **Yamamoto, M., Suwa, Y., Sugiyama, K., Okashita, N., Kawaguchi, M., Tani, N.,**
725 **Matsubara, K., Nakamura, A. and Seki, Y.** (2020). PRDM14-CtBP1/2-PRC2
726 complex regulates transcriptional repression during transition from primed to naïve
727 pluripotency. *J Cell Sci* **133**, 1–13.
728 **Zhang, B., Zheng, H., Huang, B., Li, W., Xiang, Y., Peng, X., Ming, J., Wu, X., Zhang,**
729 **Y., Xu, Q., et al.** (2016). Allelic reprogramming of the histone modification
730 H3K4me3 in early mammalian development. *Nature* **537**, 553–557.
731 **Zhang, T., Zhang, Z., Dong, Q., Xiong, J. and Zhu, B.** (2020). Histone H3K27
732 acetylation is dispensable for enhancer activity in mouse embryonic stem cells.
733 *Genome Biol* **21**, 1–7.
734
735

736 **Author Contributions**

737 Y.S. conceived the study and experimental design, performed experiments and wrote the
738 manuscript. K.S., K.Y. and N.H. performed most experiments. R.M. M.M., A.S. and Y.M
739 performed some experiments. K.S., K.Y. and N.H. contributed equally to this work.

740

741 **Acknowledgements**

742 We thank all members of Seki laboratory for stimulating discussions. This study was
743 supported by JSPS KAKENHI Grant Numbers JP18H02422, JP20H05375, JP22H04682
744 and a Special Research Grant for Individual Researchers from Kwansei Gakuin
745 University.

746

747 **Conflict of interest**

748 The authors declare no competing interests.

749

750 **Data availability**

751 RNA-Seq data has been deposited in Gene Expression Omnibus (GSE253944)

752

753

754

755